The Calibration of *ERS-1* Satellite Scatterometer Winds

D. OFFILER

Meteorological Office, Meteorological Research Flight, Farnborough, United Kingdom

(Manuscript received 1 July 1993, in final form 22 November 1993)

ABSTRACT

During the period mid-September to mid-December 1991, the RENE-91 campaign took place off the coast of Norway. Extensive in situ measurements of winds and waves were made from several platforms in order to calibrate these parameters derived from radar instruments on board the *ERS-1* satellite. Over several weeks the U.K. Meteorological Research Flight C-130 aircraft measured low-level winds beneath the scatterometer swath. Together with data from other aircraft, ships, and buoys, an objective analysis scheme was used to form the best estimate of the local wind field for a quick-look comparison with the *ERS-1* scatterometer data, and later to determine an optimized relationship between the scatterometer's backscatter values and the local wind vector. The wind fields have also been used to verify the performances of various candidate C-band radar backscatter models in retrieving wind vectors from the original *ERS-1* scatterometer data. This analysis showed that the prelaunch model could be significantly improved upon, and a new model has been selected for operational fast delivery processing. Typically, the scatterometer accuracy is about, or better than, the instrument specification of 2 m s^{-1} and 20° rms when compared with analyzed RENE-91 or operational global NWP wind fields.

1. Introduction

The European Space Agency (ESA) launched its first remote-sensing satellite, *ERS-1*, on 17 July 1991. It carries both active microwave systems—a radar altimeter (RA) and the Advanced Microwave Instrument (AMI), which is a combined wind and wave scatterometer plus Synthetic Apperture Radar (SAR)—and a passive infrared Along-Track Scanning Radiometer (ATSR) with a nadir-only viewing microwave radiometer component. The *ERS-1* mission, instrument payload, ground processing, and calibration have been described in various articles in a special issue of the ESA Bulletin (Battrick and Guyenne 1991).

The wind scatterometer is of interest to operational meteorological centers for its potentially high-quality, global coverage of surface wind vector over the oceans. The geophysical product specification, based on WMO and user requirements, is for wind speeds to 2 m s^{-1} rms (or 10%, whichever is higher) and to 20° in direction, this accuracy to be met over the range 4–24 m s^{-1}. This specification is essentially the same as that defined for the Seasat scatterometer (Grantham et al. 1977). However, being the first such instrument in space using C-band frequencies (5.3 GHz), the detailed relationship between the surface wind and backscatter (known as σ^0) was not well known prior to launch. Various methods for calibration had previously been proposed, including the use of buoys and aircraft in a dedicated campaign, conventional synoptic marine observations, and numerical weather prediction (NWP) analyses (Hunt 1986).

During the period 16 September to 10 December 1991, ESA coordinated a campaign to assist in the geophysical calibration of wind and wave products derived from the *ERS-1* satellite. The campaign, known as RENE-91, involved making in situ measurements off the coast of Norway in the Haltenbanken area using a variety of platforms, including buoys, ships, and aircraft. During this period, the satellite was in its "commissioning orbit" phase with a 3-day repeat cycle.

For a period of three weeks at the beginning of the campaign, and for nearly two weeks at the end, the U.K. Meteorological Research Flight (MRF) C-130 instrumented aircraft was based in Trondheim, the campaign's operations center. During this time, low-level measurements of the winds were made over the Haltenbanken area when the *ERS-1* scatterometer was also operating.

Data from most of the platforms participating in the campaign, together with independent objective analyses made by the Norwegian Meteorological Institute (DNMI) and *ERS-1* fast-delivery products, were made available to a local database, generally within 24 h of their measurement time. This database was used to form "best-estimate" wind fields around the Haltenbanken area, which could be used to (i) quickly compare with the *ERS-1* winds for day-to-day quality monitoring, (ii) form a high-quality dataset that could be used for calibrating or tuning the scatterometer wind retrieval algorithms, and (iii) validate such tuning.

Corresponding author address: David Offiler, Meteorological Research Flight, Building Y46, DRA Farnborough, Hampshire, GU14 6TD, United Kingdom.

2. The *ERS-1* wind scatterometer

The wind scatterometer (SCATT) on *ERS-1* measures the returned radar power in terms of the "normalized backscattering cross section," or σ^0—as defined in Long (1988)—from three antennas that form a swath to the right side of the satellite ground track (as shown in Fig. 1). The fore, mid, and aft beams point at an azimuth of 45°, 90°, and 135° to the satellite heading, respectively. The incidence angles of the radar beams—measured from the local zenith—cover the range 17°–46° for the midbeam and 25°–57° for the fore and aft beams.

As the satellite travels forward at 6.7 km s^{-1}, the three beams sweep out a swath 500 km wide; after a few minutes (depending on the position across the swath) a particular point on the surface will be illuminated by the three beams in turn. Ground processing resamples the raw radar return signal into earth-located cells or nodes of nominal size 50 km × 50 km, and with a node separation of 25 km both along- and across-track. This results in 19 nodes across the swath, the inner node edge having an offset of 225 km from the subsatellite point. By using a set of ground transponders and the azimuthally homogeneous Amazon rainforest (ESA 1988), the three averaged radar returns per cell can be calibrated into absolute σ^0 values. The AMI instrument, of which the SCATT is a part, is described more fully by Attema (1991). The major differences from the experimental *Seasat-A* Satellite Scatterometer (SASS) flown in 1978 (Grantham et al. 1977) are that SCATT has three antennas, to improve the wind direction retrieval, but only has a single-sided swath. Also, the radar signal processing is by conventional short-pulse range gating, rather than the long-pulse Doppler-gating used by SASS.

From launch until mid-December 1991, *ERS-1* was in the so-called commissioning phase orbit; at a nominal mean height of 785 km, and 98° inclination, the ground track repeated exactly (within 1 km) every 3 days. The mean equator crossing time (descending, or southbound) is 1030 local solar time.

3. C-band model transfer function

At microwave frequencies, backscattering is due principally to in-phase reflections from a rough surface; for the ocean, and at C band (5.3 GHz for SCATT), this arises from small ripples of 3–4-cm wavelength generated by the instantaneous surface wind stress. Unfortunately, theoretical considerations for the scattering of microwave radiation from the ocean surface are not sufficiently well understood to predict the backscatter to an accuracy required for practical wind retrievals. We therefore rely on empirical relationships derived from actual measurements, for instance the SASS-1 relationship developed for the Seasat scatterometer (Schroeder et al. 1982), and the later SASS-2 or Wentz model (Wentz et al. 1984). Such models are potentially subject to later improvement as more data become available (e.g., Woiceshyn et al. 1986).

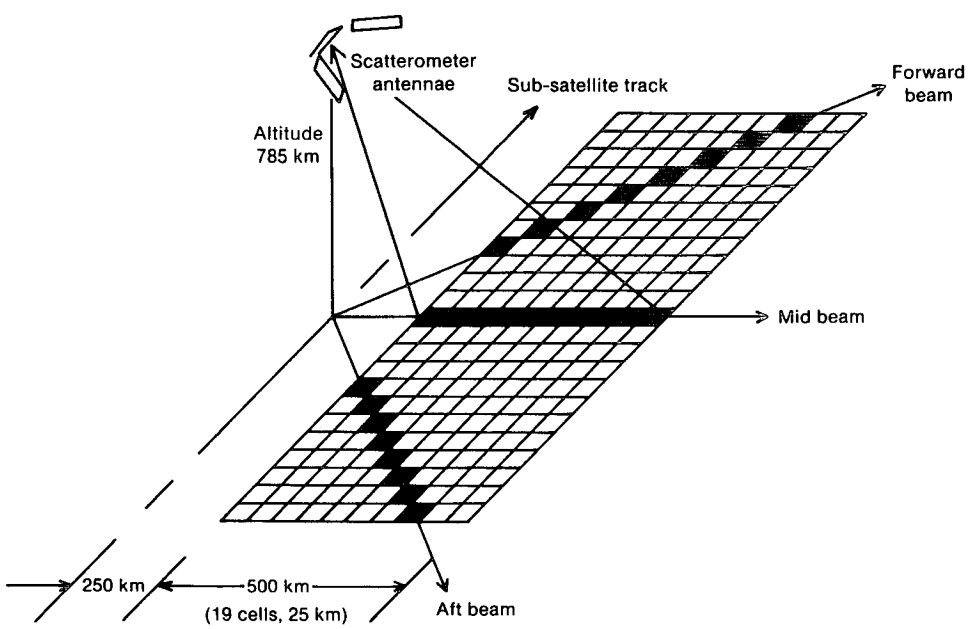

FIG. 1. *ERS-1* wind scatterometer geometry. For clarity, the 500-km-wide swath is shown as ten non-overlapping cells. In reality, there are 19 cells across the swath, on a 25 km × 25 km grid, each one being 50 km × 50 km in size.

For a given viewing geometry and surface conditions, the ocean backscatter varies with radar frequency and polarization (Jones and Schroeder 1978). The Seasat scatterometer operated in Ku-band (14.6 GHz), so SASS-1 is not valid for the *ERS-1* SCATT. During the mid-1980s, ESA coordinated several campaigns in which σ^0 measured from airborne scatterometers could be related to in situ wind observations (Attema 1986). From these campaign data, Long (1986) derived an empirical model transfer function (MTF) at C band, known as CMOD1. Later campaign data from the Mediterranean has resulted in a modified MTF known as CMOD2. This latter model has a relationship of the form

$$\sigma^0 = b_0(1 + b_1 \cos\phi + b_2 \cos 2\phi), \quad (1)$$

where

$$b_0 = 10^{\alpha} U^{\gamma_0} \quad (2)$$

and the coefficients b_n, α, and γ are dependent on the incidence angle; U_{10} is the wind speed (at a height of 10 m and assuming a neutrally stable boundary layer). Here, ϕ is the wind direction relative to the azimuth look direction of the radar beam; this is defined such that $\phi = 0°$ is looking upwind, 180° is downwind, and 90° is crosswind. This MTF is plotted in Fig. 2 to show the relationship of σ^0 as a function of ϕ for a number of constant wind speeds.

CMOD1 and later CMOD2 were used to develop algorithms to retrieve winds from simulated triplets of σ^0 and to remove the inherent directional ambiguity resulting from the $\cos 2\phi$ term in (1) (Cavanié and Offiler 1986). CMOD2 was implemented in ESA's operational wind retrieval scheme for generating the fast-delivery (FD) wind products after launch.

In general, the retrieval algorithms work by calculating a "cost function" or weighted residual, which in its simplest form can be the rms difference between the measured backscatter values, $\hat{\sigma}^0$ and the MTF-predicted values, $\sigma^0(\ )$:

$$R = \{\sum_{i=1}^{3} [\hat{\sigma}_i^0 - \sigma^0(U', D' - \phi_i, \theta_i)]^2\}^{1/2}, \quad (3)$$

where U' and D' are the current estimates for wind speed and direction, ϕ_i is the radar beam azimuth angle (from north), and θ_i the incidence angle for beam i. The resulting residual R is minimized by adjusting the values of U' and D'. It is beyond the scope of this paper to describe the many different mathematical techniques that can be used to achieve this (see, e.g., Chi and Li 1988).

Depending upon the surface conditions and the detailed form of (3), there may be from two to six local minima in R, called "solutions" in (U, D). One of these solutions will be "correct," and a second solution, roughly 180° away, will have a similar residual value.

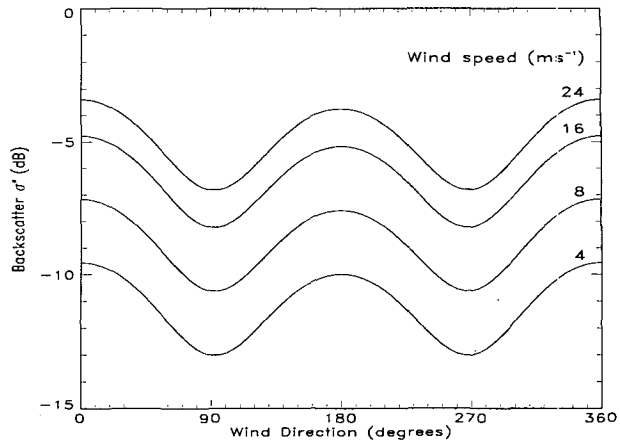

FIG. 2. Backscatter σ^0 defined by the CMOD2 transfer model, as a function of relative wind direction for different wind speeds (5.3 GHz, vertical polarization, 30° incidence angle).

Any other minima will usually have much higher residuals and small probabilities of being correct. For CMOD2 with simulated noisy σ^0 values, the difference between the upwind and downwind peaks seen in Fig. 1 meant that the solution with the smallest residual would be correct on around 70% of cases. Further ambiguity removal using internal consistency checks on the 2D swath could raise the probability of identifying the correct solution to 95% (Offiler 1985).

However, the performances of these algorithms are critically dependent on the accuracy of the MTF in predicting the measured σ^0 for given surface conditions. In particular, prior to launch, there was uncertainty in the applicability of CMOD2—derived from aircraft scatterometer measurements—to measurements from space, partly because of the vastly different instrument "footprints" (a few hundred square meters for an aircraft, 2500 km^2 for the SCATT).

4. The RENE-91 campaign

One of the goals of the RENE-91 campaign was to validate the performance of the CMOD2 model in terms of both predicting the σ^0 values actually measured by SCATT and the quality of the winds retrieved from them. If necessary, the model's coefficients or the model formulation itself could then be tuned so that the wind product specification could be met. It should be stressed that we are concerned here only with *geophysical* calibration; it is assumed that the *engineering* (σ^0) calibration is correct.

a. Reference-level winds

The scatterometer-derived wind speeds are specified to be those equivalent to a measurement at a reference height of 10 m in a neutrally stable atmosphere (U_{10}). To compare—and geophysically calibrate—the scat-

terometer winds, all the measurements were required to be of the same quantity. For the in situ data, each experimenter adjusted their sensor-level winds to U_{10} prior to delivery to the central campaign database. This was achieved using a common boundary layer model proposed by Ezraty (1985).

In this model, the wind profile is assumed to take the form

$$u(z) = \frac{u_*}{k}\left[\ln\left(\frac{z}{z_0}\right) - \Gamma\left(\frac{z}{L}\right)\right] \tag{4}$$

where $z_0 = 0.0185u_*^2/g$ is the surface roughness length as proposed by Wu (1982), and u_* is friction wind velocity, k is von Kármán's constant (0.4), L is Monin–Obukhov stability length, g is acceleration due to gravity (9.8 m s^{-2}), and z/L is dimensionless stability length.

Here, Γ represents a stability-dependent modification to the logarithmic profile:

$$\Gamma = \begin{cases} -5z/L, & \text{for } z/L > 0 \text{ (stable conditions)} \\ 0, & \text{for } z/L = 0 \text{ (neutral conditions)} \\ 2\ln\left(\dfrac{1+X}{2}\right) + \ln\left(\dfrac{1+X^2}{2}\right) \\ \quad - 2\tan^{-1}(X) + \dfrac{\pi}{2} \\ \quad \text{with } X = (1 - 16z/L)^{1/4}, \\ \quad \text{for } z/L < 0 \text{ (unstable conditions)} \end{cases} \tag{5}$$

(see, e.g., Large and Pond 1982). Here, z/L is a function of air–sea temperature difference and wind speed, with corrections for humidity and bulk estimates of the temperature and humidity fluxes. The Ezraty model is valid only for $-1.0 < z/L < 0.5$.

Similar relationships are used for the temperature and humidity profiles. Since these profiles in turn control the atmospheric stability, and hence u_* by means of (4), an iterative procedure is applied that generally converges quickly. If the model fails to converge within a limit on the number of iterations, or z/L is outside the bounds −2.0 to 1.0, then the algorithm sets z/L to zero, and the model is rerun for neutral conditions, and the condition flagged. This occasionally happened for aircraft measurements above about 800 m when the flight-level winds are not well related to the surface boundary layer.

The Ezraty model has been used in previous campaigns, and its use and limitations are discussed by Daniault et al. (1988).

b. C-130 wind measurements

Depending on the needs of particular experiments, the MRF C-130 can carry a wide range of instruments for measuring various atmospheric parameters, including chemistry, radiation—in the infrared and microwave—clouds, and aerosols (Readings 1985). However, for deriving winds, only the standard sensors are required; these include the Inertial Navigation System (INS) (giving aircraft's 3D position, attitude, and heading), wind vanes (for angle of side slip and angle of attack), and dynamic (pitot) pressure for airspeed. In addition, to derive the most accurate winds, additional measurements are made using other navaids such as the Global Positioning System (GPS), Omega, Decca, and Doppler radar. These other navaids—in particular GPS—are used during ground processing to correct for INS drifts and Schuler oscillations to obtain the most accurate aircraft ground velocities.

Also, compensated air temperature, dewpoint, static pressure, surface temperature (from a broadband infrared radiometer) and radar altimeter heights (up to 1500 m) are measured. The dynamic pressure, true air temperature, and static pressure are used to derive the true airspeed. The wind speed and direction can then be calculated by the vector difference of ground and air velocities (Axford 1968). On an error budget analysis, it is expected that the flight level wind can be determined to approximately 0.5 m s^{-1} (rms vector error). Assuming equal rms errors in each wind component, this is equivalent to about 0.4 m s^{-1} in scalar wind speed and under 10° in wind direction.

For the C-130 data, full atmospheric compensation was applied to the derived flight-level wind speeds using the flight-level temperature, humidity, and static pressure, radiometric sea surface temperature, and calculated temperature lapse rate in order to derive the U_{10} wind speed with the Ezraty boundary layer model described above.

Because the aircraft parameters are logged at different rates (from 1 to 32 Hz) all were first averaged over equivalent 5-km lengths of flight track (50 s at a nominal flight speed of 100 m s^{-1}), and various quality control criteria applied. The temperature lapse rate was calculated from the last aircraft profile, usually from 1500 to 15 m. Although some profiles showed highly nonlogarithmic wind speed variation with height, such deviations were generally above the nominal flight level of 70 m, and are not thought to contribute significant error to the derived U_{10}. The wind direction at 10 m is assumed to be the same as that at the flight level; the C-130 profiles confirmed that this was usually the case in the lowest 200 m of the atmosphere, and no systematic turning of wind direction with height was observed.

All data processing, involving quality control, full sensor calibrations, INS corrections, derivations of averaged U_{10}, and formatting, was done at the campaign headquarters following each flight. The final datasets were delivered to the local database in Trondheim the day following a flight.

c. C-130 aircraft missions

While *ERS-1* was in its commissioning phase 3-day orbit, scatterometer passes were scheduled to give good coverage of the Haltenbanken area three times every 3 days, with other passes dedicated to SAR wave measurements. The C-130 flew missions on two of these opportunities in each 3-day cycle during the periods 18 September–4 October and 30 November–9 December 1991 inclusive. The satellite passes were the "day 1" southbound pass at around 1050 UTC and the "day 2" southbound pass at around 1015 UTC. Each flight covered as much of the swath as was practical, underflying all incidence angles and a length of the swath sufficient to determine the two-dimensional wind field. Figure 3 gives an example flight track and the derived winds for a day 1 pattern. The nominal flight altitude was 70 m, with a profile between 1500 m and 15 m at each corner of the pattern, and passing over at least two buoys (locations marked "T10," "T9," and "T1," in this case) for cross comparison. All tracks were flown clockwise around the pattern.

The typical flight duration was around 6 h, so there is obviously a time difference between some of the aircraft and scatterometer measurements; the flight was planned so that the C-130 would be over the buoy position T1 at the time of the *ERS-1* overpass. On the day 2 passes, the swath was closer to the coast and further north. On these flights, the rendezvous point was T10, traveling up-swath.

In all, 18 successful flights were made when good data were obtained; on two other flights, the INS drifted

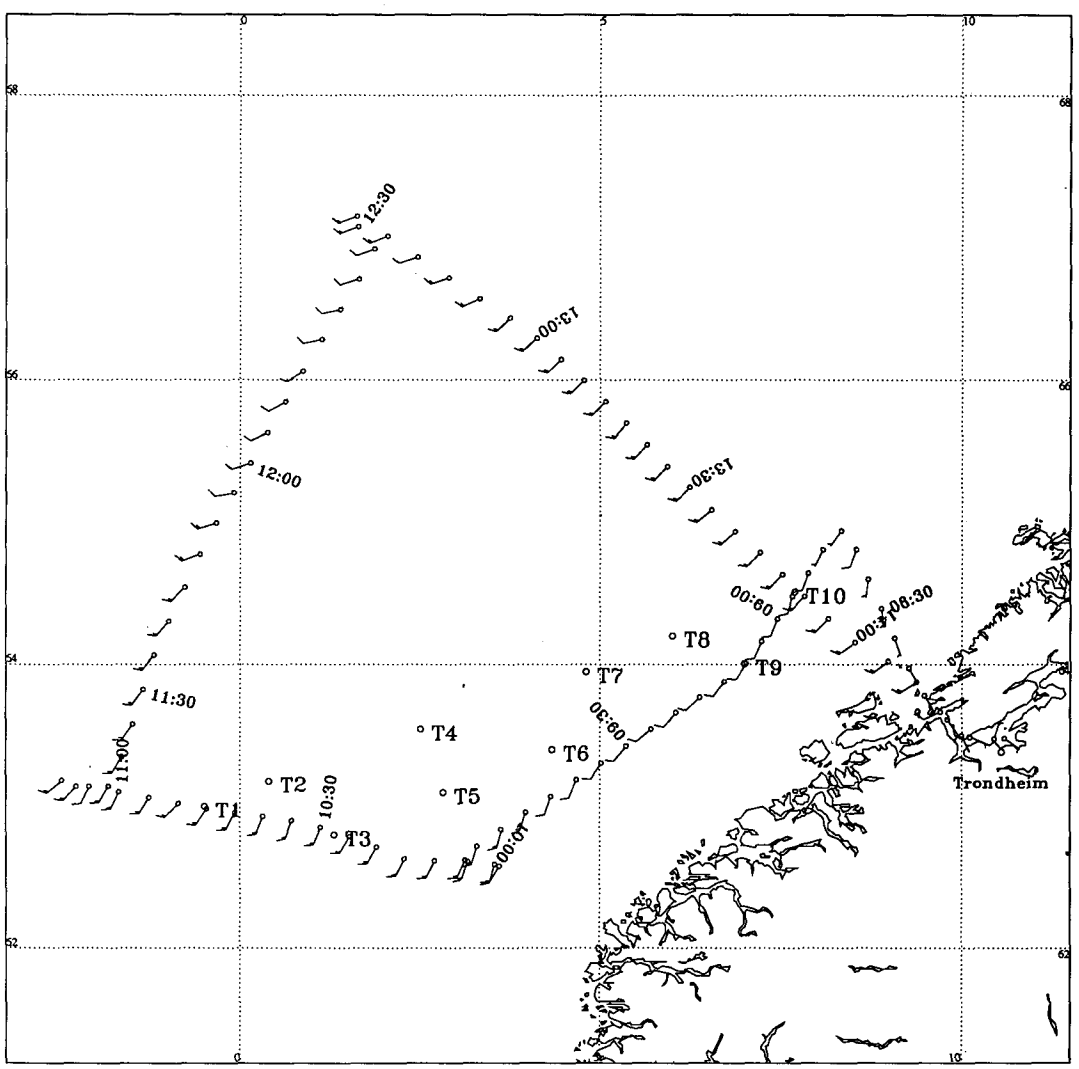

FIG. 3. Example C-130 flight track and derived 10-m winds for 0830–1400 UTC 2 December 1991. The wind symbols are plotted conventionally, with each full feather representing 10 m s^{-1}. The positions of the Tobis buoys are indicated by the points labeled T1–T10.

badly, and although the aircraft position could be recovered with the GPS, the aircraft velocities could not be derived with sufficient accuracy to obtain reliable winds. Only one planned mission was not flown because of engine problems. Over 100 h of data gathering were obtained during the campaign.

d. *Other data sources*

To maximize the spatial and temporal coverage of in situ wind measurements, and to lessen the risk associated with just one sensor type, the RENE-91 campaign coordinated the use of the following data sources for winds: aircraft—C-130 (U.K.), Do-228 (Germany), and Merlin IV (France); radar—RACS (on Do-228) (Germany); buoys—10 Tobis-3 buoys (Norway, France); ships—OWS *Mike* (Norway), R/V *Gauss* (Germany), *Håkon Mosby* (Norway); platforms—Gullfax (Norway); and models—NWP wind field analyses (Norway, ECMWF)

Except for the Merlin aircraft, which mainly flew at high level with a wave-measuring scatterometer, all of these sources provided U_{10} wind speeds or sensor-level measurements that were converted to U_{10} using the Ezraty boundary layer model. Each data source is complementary in that they are made at many different locations over the analysis area and by different sensor and sampling systems. Of course, not all sources are available for every scatterometer pass; this was particularly true for the Tobis buoys, which failed to provide any usable data until late into the experiment. Generally, data were available to the campaign database, in a common format, within a day of measurement.

The RACS data were taken on the Do-228's outward leg at high level (4000 m), and the Do-228 winds were those derived directly from the aircraft navigation system on the return at low level (100–200 m); no postflight corrections were applied other than the conversion to U_{10}. Thus the two sets are not simultaneous. On a small number of occasions the C-130 and Do-228 both passed over the nominal position of buoy T1 within a minute of the satellite overpass; at these times, the winds agreed to about 1 m s^{-1} and 10°. Comparisons between the Do-228 navigation winds and those derived from the RACS show a similar level of agreement (Wismann 1992).

Several other platforms made wave measurements with various types of sensors, in support of the *ERS-1* wave mode scatterometer and radar altimeter, but are not considered further for this study.

5. RENE-91 analyses

a. *Analysis method*

When comparing meteorological satellite data with in situ measurements, it has been traditional to use one of the following two methods:

(i) Collocate one in situ measurement with one or more nearest satellite point and within some time limit—on an essentially one-for-one basis—for instance as used by Offiler (1984) in analyzing the performance of the SASS. This method has the disadvantage of introducing collocation errors because of spatial or time differences, and also of not comparing like with like, since the in situ measurement is usually taken as a time average at a point, and the satellite is an areal average at an instant in time. Such collocations or "hits" tend to be few in number and rarely cover the whole range of desired parameters.

(ii) Some of the above disadvantages can be reduced by first assimilating the many varied forms of available in situ data into numerical weather prediction (NWP) models or sophisticated large-scale planetary boundary layer (PBL) models (Brown et al. 1982) and interpolating the required parameter from the analysis grid to the satellite footprint location. However, such models tend to have rather coarse horizontal resolution compared to that of the satellite, and are generally tuned to the synoptic scale. They tend to smear out or miss small-scale features that might be represented in the satellite swath. In the case of the RENE-91 campaign, the in situ data, although gathered quickly by campaign standards, could not delivered to weather centers in time for their NWP operational model runs, so this collocation method could not be used during the campaign.

For this campaign, a compromise solution was used; a single-variable, two-dimensional objective analysis scheme based on a recursive filter technique as described by Hayden and Purser (1988). The analysis scheme was tuned to use all available RENE-91 in situ winds, with the Norwegian Meteorological Institute (DNMI) wind fields as a background "filler" out to the edge of the analysis area to minimize grid boundary initialization errors. A 25-km grid size was chosen as comparable with the scatterometer node spacing, with the grid covering the area 60°–70°N, 5°W–15°E. Because all the RENE-91 datasets were supplied in a common format, winds from all available sources could be incorporated into the analysis simply; the actual sources and quantities varied from day to day. Isotach analyses—the so-called triangle fields—were also made from JASIN (Joint Air–Sea Interaction Program) in situ winds for comparison with SASS (Brown et al. 1982), but this was on a coarser grid (60 km) and had far fewer observations (8 platforms). A debatable point is that the complete JASIN dataset was referenced to a single buoy, with consequent uncertainties in the biases. No such assumptions were used in the present analyses.

Each data source is assigned a relative weight depending on its perceived a priori quality; for instance most of the in situ data is weighted with values 8–10, but the DNMI background (which should not signif-

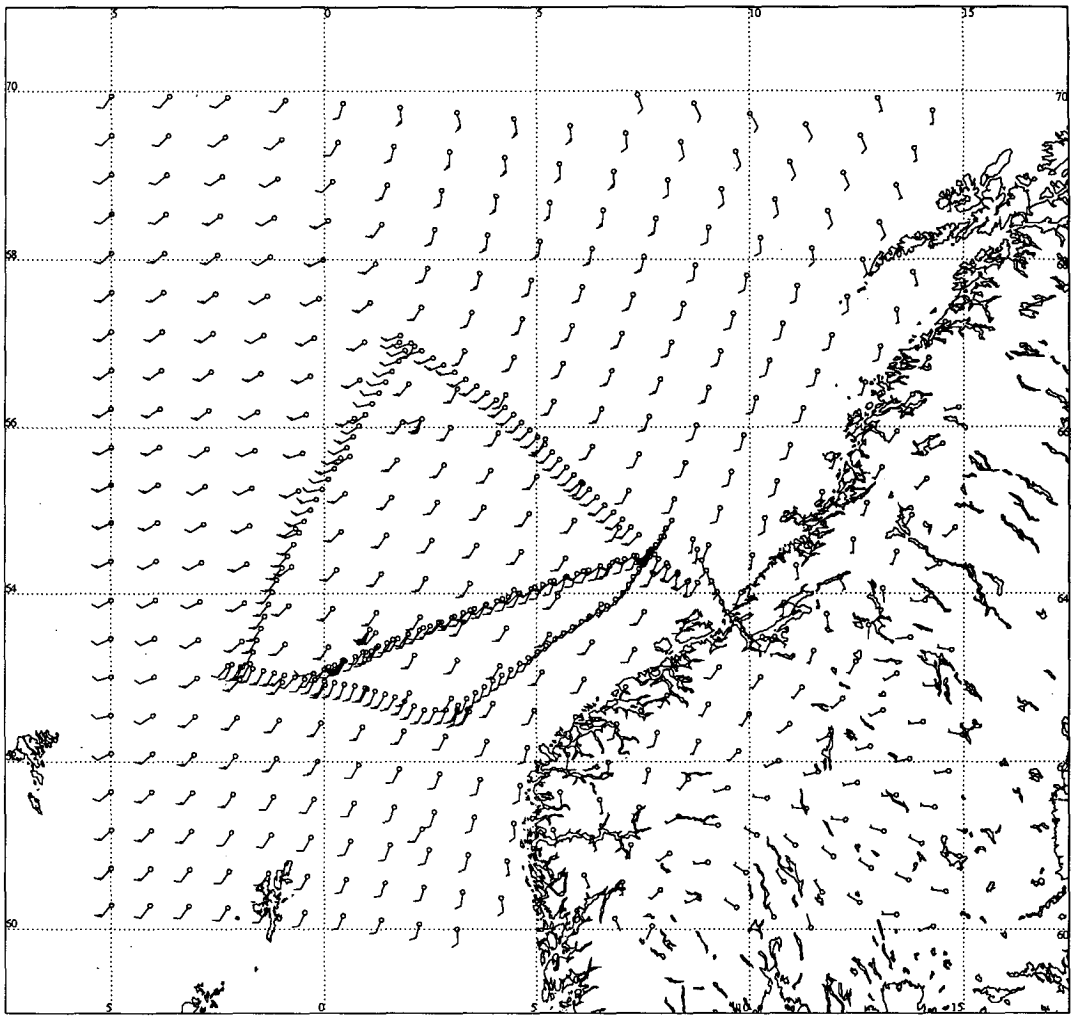

FIG. 4. Sources of RENE-91 wind data in the Haltenbanken area within 3 h of the *ERS-1* overpass at 1049 UTC 2 December 1991.

icantly influence the analysis in the presence of in situ data) is weighted at 1. In addition, the weighting value is reduced by an amount depending on the time difference of the measurement from the scatterometer overpass time and also by an amount related to the altitude of the platform (for aircraft). These weights are such that data more than 3 h from the satellite pass or when an aircraft was above 700 m are not used. For the Tobis-3 buoys (which have redundant wind sensors), where both lower and upper sensors were available, the one with the smallest variability has been used.

The analysis software also calculates a "quality index" (QI); this is a number scaled to be in the range 0–100, and at each grid point is combined measure of (i) the expected errors of individual data sources contributing to that grid point, (ii) individual observation weightings (due to the time difference from satellite overpass time, or due to aircraft altitude), (iii) the local density of observations, and (iv) the local consistency between observations. The higher the QI value, the higher the *confidence* in the analysis. The relative source weightings were also chosen such that a QI value of around 5 is a rough threshold where higher values indicate that the in situ winds have influenced the analysis, and lower values that only the DNMI background has been used. The quality index by itself is not necessarily an indication of the *accuracy* of the analyzed winds (but see the results in section 6c).

Figure 4 shows an example of the data inputs for one analysis. In this case, the C-130 track from Fig. 3 is seen, as is the Do-228 track through the center of the C-130 loop. This track actually contains RACS winds outbound and Do-228 navaid winds back. This analysis also uses winds from three Tobis-3 buoys, OWS *Mike* (just below the northernmost part of the C-130 track), and the Gullfax platform to the south.

The slightly sloping grid shows the midday DNMI NWP background wind field.

The advantages of this analysis method are that (i) it minimizes errors in any one platform or in an individual observation, (ii) there is reduced likelihood of any systematic errors or biases, (iii) the spatial average is more comparable to a scatterometer measurement and (iv) it maximizes the number of collocations, particularly by covering the whole width of the swath and sampling along swath—although there will still be a tendency to smooth very small-scale features or sharp gradients over one or two grid lengths, or where there are rapid changes in time.

The accuracies of the analyzed winds are difficult to assess due to the lack of any other independent quality data. However, in the areas where QI > 5, the quality of the analyses will be highly dependent on the accuracy of the in situ data, and section 4d suggests these to be the order of 1 m s^{-1} and 10°. Here, the DNMI background winds do not greatly influence the analyses, though they dominate outside these regions. When attempting to use the DMNI fields to extend the wind information away from Do-228 tracks, Wismann (1993) found only 14 out of 46 fields agreed sufficiently well with the aircraft underflights to be useful. The main problems were found to be (i) often in southwesterlies, a strong low-level coastal jet was present in the Do-228 and C-130 data, not represented at all in the DNMI fields and (ii) individual differences of up to several meters per second and large directional differences associated with cyclonic and frontal synoptic situations. These are attributable to the relatively low resolution of the NWP analyses (on 50-km grid, the effective resolutions being 100–200 km). The DMNI fields were also based on the sparse synoptic data in this area that were available in near-real time. These problems are such that DNMI fields are not of sufficient quality—on the small scales required here—to directly validate or calibrate the *ERS-1* scatterometer. The dedicated analyses, as described above, are the statistical "best fit" to *all* the data sources, and are probably the most representative estimate of the "true" *neutral stability* winds on the spatial scale of the scatterometer cells (where QI > 5), and in most cases we believe they will be within ±1–2 m s^{-1} and ±10°–20°—that is, better than the accuracy required of the scatterometer. For comparison, Brown et al. (1982) estimate their JASIN triangle fields' accuracy to be ±1 m s^{-1} and ±15°, with the large-scale PBL fields to be, at best, ±2 m s^{-1} and ±15° in homogeneous areas. An indirect estimate of the RENE-91 analyses is discussed with the summary of results in section 6c.

Finally, the analyzed winds are bilinearly interpolated from the four surrounding grid points to each of the *ERS-1* SCATT cell locations within the grid's area. Figure 5 shows the RENE-91 analysis made using the data in Fig. 4 together with the *ERS-1* FD winds. The contour is the QI = 5 value, inside which the analysis is dominated by the in situ measurements, and outside is influenced only by the DNMI background wind field. Over most of the swath, the scatterometer shows good agreement with the analysis except in the NW part of the contour, where there are differences in wind direction of 20°–30°; this is probably due to an active front passing through the area between the time of the satellite pass and the C-130 track 1–2 h later. The frontal position can be identified from the wind direction changes in Fig. 3 along the northeast- and southeast-bound C-130 legs.

Within days of the start of the campaign, we noticed that there was a large, consistent difference between the RENE-91 analyses and the SCATT wind directions. This was notified to ESA; within the week, an error had been found in the FD processing software and corrected. This illustrates the value of having rapid data delivery and on-line access to common-format files, together with appropriate analysis tools, for campaigns of this type.

b. *Summary of analyses*

Since the end of the campaign, ESA has implemented several software modifications and updated the engineering calibrations. Most of the SCATT data gathered during RENE-91 have been reprocessed from the original telemetry tapes. These reprocessed data have been merged with the RENE-91 analyses to update the collocations files. The results described below refer to these reprocessed data. These collocation files (which include the measured σ^0 values and associated parameters, as well as FD winds and the RENE-91 collocated analyzed winds) have also been delivered to the *ERS-1* database in the agreed format for use by other groups.

A total of 81 scatterometer passes have now been collocated with analyses made using the technique described above, creating nearly 22 000 individual (but not totally independent) collocations with a QI ⩾ 5. Not all of these passes have good coverage of in situ data, and not all have DNMI backgrounds available, but the QI value is a good filter for poorly covered cases. Some cases, like the one shown in the figures, have frontal systems that may give rise to "errors" in the analyses—these may need to be excluded by inspection of the data and by consulting the synoptic patterns analyzed by DNMI (which are available as part of the campaign operations documentation) before being used for optimal calibration purposes. However, the statistical analyses presented here have used all available passes, since the scatterometer wind processing must cope with all types of synoptic situations in operational use.

These analyses cover the wind speed range 1–21 m s^{-1} with a distribution peak at 8–9 m s^{-1}. Synoptic wind directions are mainly from southwesterly through to northerly, but as the *ERS-1* passes are both ascending

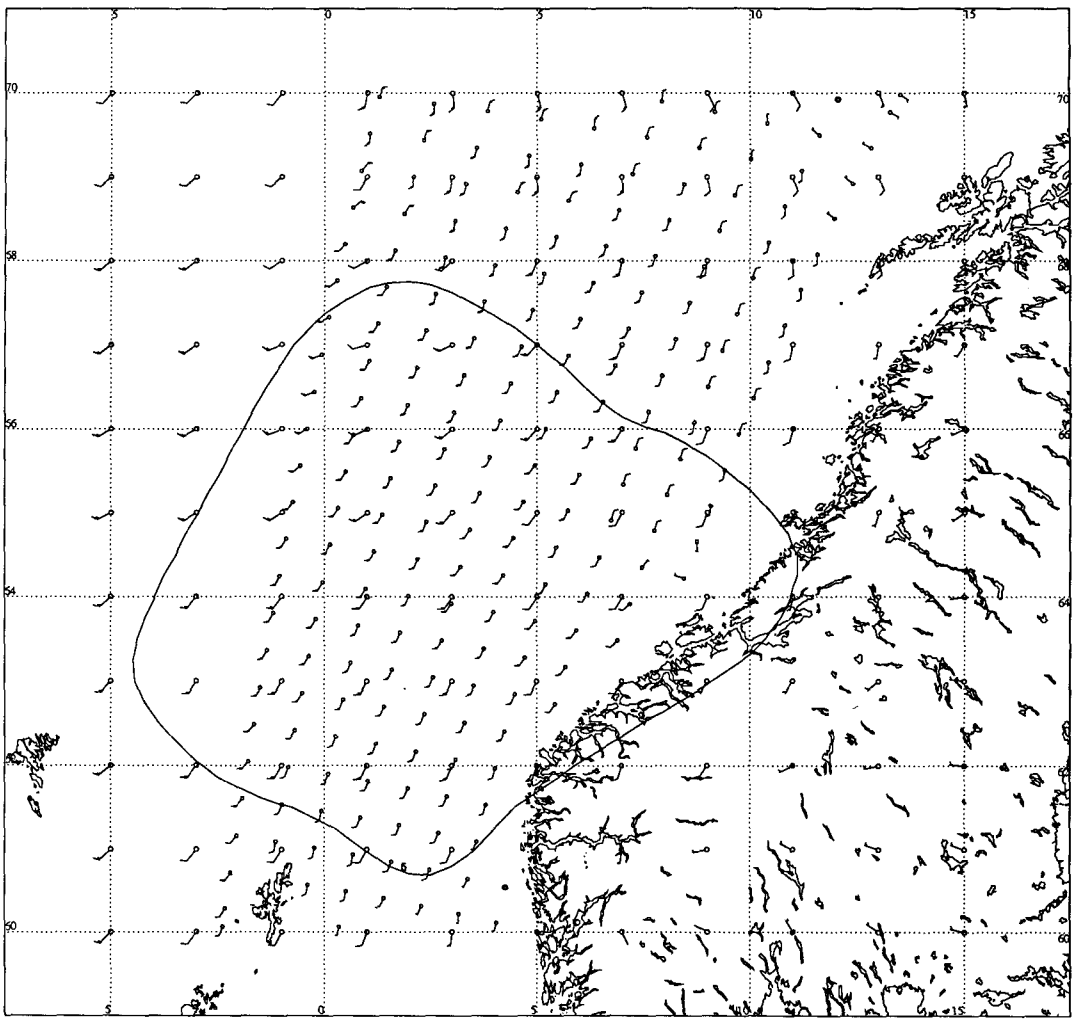

FIG. 5. Scatterometer-derived winds and RENE-91 analysis for the *ERS-1* overpass time of 1049 UTC (at buoy T1) on 2 December 1991. For clarity, only alternate SCATT cells and every fourth grid point of the analysis have been plotted. The contour is for a quality index (QI) value of 5.

and descending, and three scatterometer beams cover 90° in azimuth, the wind directions relative to any beam have a more uniform spread. In one case, the scatterometer wind speeds derived by ESA had been set to a constant value, although the σ^0 values were valid.

Taken over the remaining 80 cases (14 300 collocations with wind speeds ≥ 4 m s^{-1} and QI > 5), the rms differences between the ESA FD scatterometer winds and the collocated analyses were the following: speed—2.7 m s^{-1}, direction—103° (values as found), direction—19° (ambiguity corrected), vector—4.1 m s^{-1}, and ambiguity removal—62% of directions within ±90° of analysis. This showed that measured against the RENE-91 analyses, although the *ERS-1* winds—with additional attention to ambiguity removal—would probably have been acceptable for NWP use, the wind vector retrieval from the CMOD2 MTF required tuning if the scatterometer specification of 2 m s^{-1} and 20° was to be met. This analysis also indicated that the FD scheme's ambiguity removal was rather poor, which was the first evidence that the assumed upwind–downwind differences in σ^0 were not as marked in practice as the MTF had assumed. (At this time, ESA was not using any background wind information for ambiguity removal; since June 1992, ECMWF forecast fields have been available to the FD scheme.)

6. Wind model tuning

a. Candidate model transfer functions

Although the global, near-real-time scatterometer winds derived using the prelaunch MTF (CMOD2) compared favorably with conventional synoptic observations from ships and buoys, some deficiencies were

clear, and ESA felt that the product was capable of improvement. Several groups, some of which were involved in the RENE-91 campaign, have used different sources of wind data either to tune the coefficients of the CMOD2 empirical relationship defined by (1) and (2), or to define a new one. These groups include ESA themselves, the European Centre for Medium-Range Weather Forecasts (ECMWF), the French Meteorological Office (Meteo-France), the French Oceanographic Institute (IFREMER), and the Universities of Hamburg (IFMEE) and Oregon. The wind data used have included the RENE-91 collocations described in this paper, subsets of the RENE-91 in situ measurements, deep-water NOAA buoys, and NWP models. Most of this work is reported by Wooding (1992), Stoffelen and Anderson (1993), and Wismann (1993). The details of each of these proposed models—the empirical mathematical function and its associated coefficients—were passed back to the U.K. Meteorological Office for independent assessment.

Each MTF has been implemented in its given analytic form with the supplied coefficients, which has then been used to generate look-up tables of σ^0 as functions of wind speed, relative wind direction, and incidence angle. The wind retrieval processing simply interpolates from one of these precalculated tables for the evaluation of the MTF residual defined by (3) for a particular run.

The retrieval algorithms used in the Meteorological Office's processing are different from those used by ESA in the FD system, but follow the general procedure outlined in section 3. For each candidate model in turn, a "batch" (the complete RENE-91 dataset or one day's worth of FD data) of measured σ^0 triplets was processed to retrieve a set of up to four ambiguous wind vectors per cell, and the "correct" vector selected by reference to the background using a probabilistic technique. This method assigns a relative probability of each solution being the correct one from a combined estimate of the errors in (i) the scatterometer, based on the residual R from (3), and (ii) the background wind direction, as a function of wind speed. This will favor, but not force, solutions with low R values or that—for higher wind speeds—are closest to the background direction, to be selected.

Finally, for each complete length of swath, a weighted modal filter was applied to ensure local consistency in the derived wind field (Offiler 1985; Cavanié and Offiler 1986). This filter also takes into account the relative probabilities of the selected solution in the neighboring cells when forming a local direction estimate. This avoids having correlated areas where the previous ambiguity removal stage may be suspect (low wind speeds and/or high residuals) from greatly influencing "good" areas when the filter is applied iteratively, while allowing such "poor" areas to be improved.

Candidate MTFs from the various groups have been tested in two phases. In the first phase, data prior to March 1992 had been used in the tuning, and data after March for the second phase. The significance of this date is that after analyzing the first few months of engineering performances, ESA introduced new calibration coefficients for σ^0 on 1 March 1992, resulting in a generally lower estimate of backscatter than previously. This in turn primarily caused a bias in retrieved wind speed; this alone required the models to be retuned. Since that date, ESA has reprocessed the original RENE-91 raw datasets to produce σ^0 values to the current calibration standard; we have used these updated files to produce new collocation sets against which we have reassessed all the candidate models.

b. *Statistical analysis*

The objective of this study was to select *the model that produces the highest quality wind retrievals,* with no explicit tests on the performance in predicting the σ^0 measured by SCATT. The criteria for "highest quality" are similar to those in validating traditional meteorological data sources, such as from ships—for example, the overall "errors" in terms of bias and standard deviation of wind speed and direction separately, or by the rms vector, when compared to the true winds. Of course, since we do not know the true winds, but only an estimate from other sources, our comparison can only be stated to be a difference from the (independent) estimate, or background. The RENE-91 collocation data has been used as the prime source of comparison information since these are felt to be the highest quality estimates of the real wind—albeit for a small area and small number of independent cases—with the global FD data acting as confirmation of model performances in the operational mode against NWP model wind analyses.

In the statistical analyses that follow, these differences are in the sense of "scatterometer minus background." Only cells having all three beams in operation, and with no land in the footprint have been included. Also, for the global FD data, a sea-ice mask has been applied to ensure that all σ^0 measurements are made over the open ocean. Additionally, data cells with QI < 5 (RENE-91 collocations only), or with background wind speeds less than 4 m s^{-1} (wind directions are not reliable at low speeds with any measurement system, including the background fields) have been excluded.

For each cell meeting these selection criteria, the statistical differences between the retrieved scatterometer wind (RET) and the collocated background (BG) are calculated. The basic statistical parameters include the mean RET minus BG (bias) in wind speed, the standard deviation of the differences (SD) in wind speed, the bias and SD in wind direction and the rms absolute vector difference. Because the models are required to perform equally well over a wide range of conditions (i.e., at least over the wind speed range 4–24 m s^{-1}, over all wind directions, and over the whole

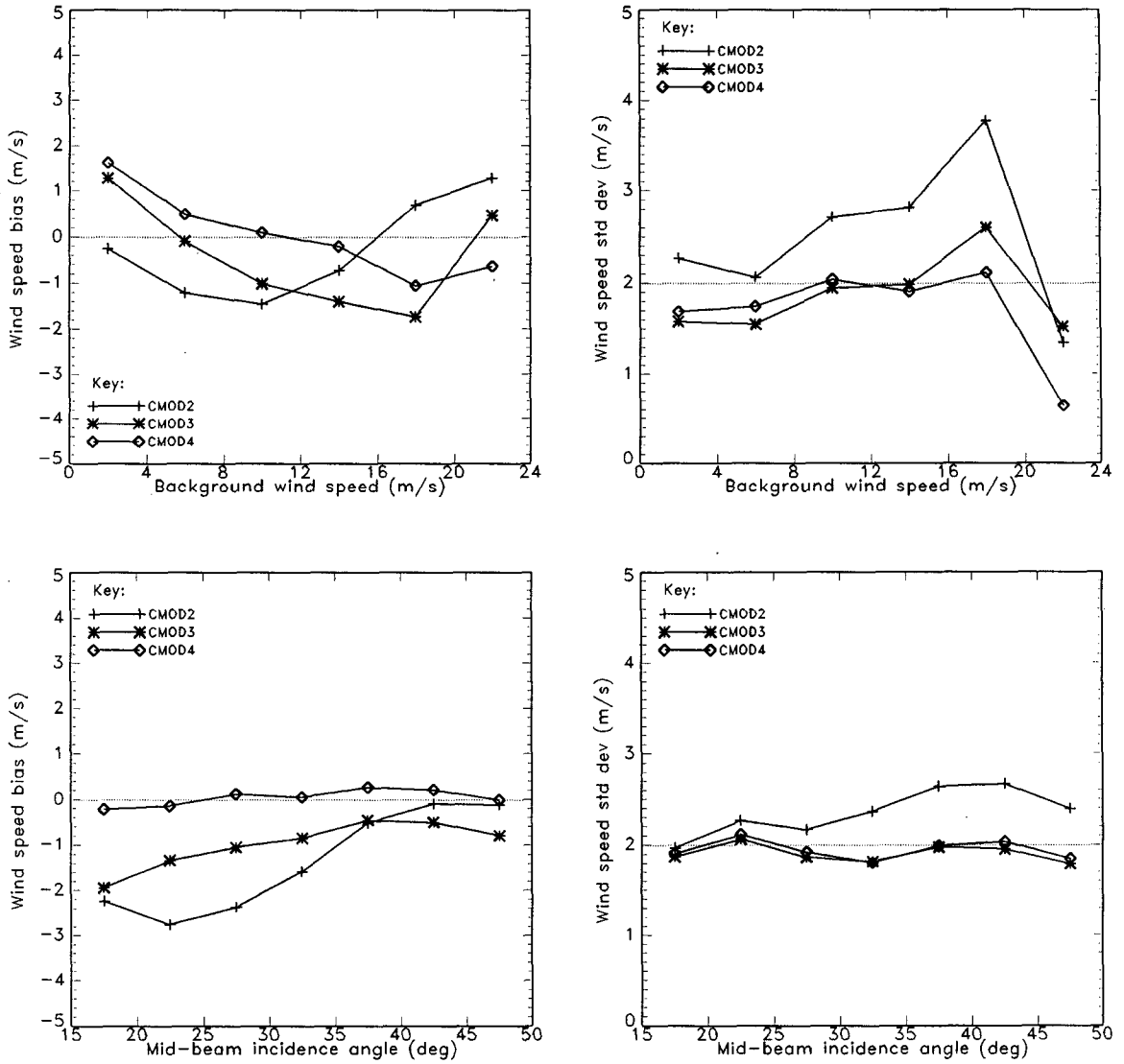

FIG. 6. Summary graphs of wind speed differences from RENE-91 analyses for various alternative wind transfer models.

width of the instrument swath), the comparison statistics have been broken down by wind speed and incidence angle to detect any trends with these parameters.

These statistics, as well as being binned, are also averaged over all incidence angles and over winds 4–24 m s^{-1}, weighted by the observation density distribution. This procedure gives most emphasis to the areas where there is most data, as would be the case if we were analyzing global ship data, for instance. However, this could favor models that retrieve well in midrange, but poorly, for instance, at high wind speeds where there are few observations; unweighted averages across all bins have therefore also been calculated.

In addition, a validation of the ambiguity removal skill using only a ranking based on the residual value R from (3) for each solution is calculated as a "percentage correct." This can be considered as a measure of the upwind–downwind ratios in the MTF. However, ambiguity removal performance was not a prime aim of the study, although this and other diagnostic parameters were assessed during the selection of candidate models.

c. *Model performances*

The performances of each of the candidate MTFs for phase I were reported and discussed at a geophysical calibration workshop (Offiler 1992). Most of the new versions improved upon CMOD2, and a short list was drawn up; the workshop recommended the model provided by ECMWF and this was implemented as

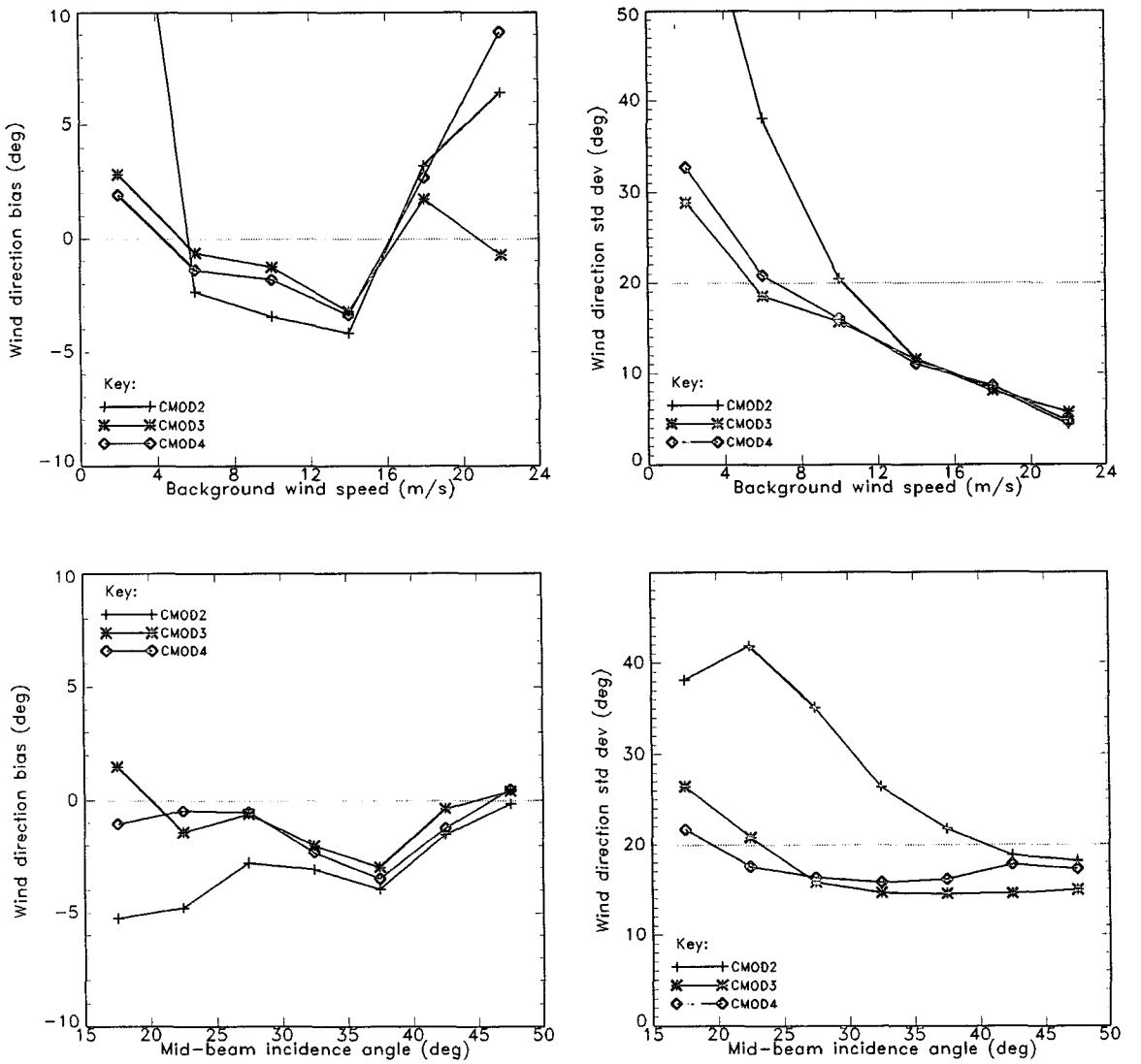

FIG. 7. Summary graphs of wind direction differences from RENE-91 analyses for various alternative wind transfer models.

CMOD3 by ESA for operational processing from 10 June 1992. This model's formulation was a little more complex than that for CMOD2, as given in (1) and (2), but was more similar to a later MTF, CMOD4 (see below).

However, the engineering calibration change that March, and the acknowledged poor fit of CMOD3 at small incidence angles and at low wind speeds required the tuning process to continue. Most of the groups that supplied models during phase I continued their tuning

TABLE 1. Summary of a comparison of *ERS-1* SCATT winds (reprocessed by the U.K. Meteorological Office) against RENE-91 analyses for each version of the operational model transfer function. Here AR is the percentage of cells correctly dealiased using only the residuals calculated by Eq. (3). (These statistics exclude winds less than 4 m s^{-1} and QI < 5.)

Model identifier	Number of cells	Speed (m s^{-1})		Direction (deg)		Vector (m s^{-1})	AR
		Bias	SD	Bias	SD	rms	(%)
CMOD2	18 878	−1.1	2.6	−2.8	26.9	3.8	52
CMOD3	18 878	−0.7	1.9	−1.2	16.5	3.1	45
CMOD4	18 878	0.1	1.9	−1.6	17.0	3.2	57

TABLE 2. Comparison of *ERS-1* SCATT fast-delivery winds (reprocessed by the U.K. Meteorological Office) against Meteorological Office global NWP analyses. Data are for 15–30 March 1992 for CMOD2 and CMOD3, and 14 October–4 November 1992 for CMOD4.

Model identifier	Number of cells	Speed ($m\ s^{-1}$) Bias	Speed ($m\ s^{-1}$) SD	Direction (deg) Bias	Direction (deg) SD	Vector ($m\ s^{-1}$) rms
CMOD2	820 374	−1.3	2.6	1.4	22.7	4.1
CMOD3	820 374	−0.9	2.2	1.1	21.1	4.0
CMOD4	1 437 910	0.0	2.1	1.2	20.9	3.6

effort; for phase II, several modified formulations and coefficients were ready to be tested by October 1992 (e.g., Stoffelen and Anderson 1993; Wismann 1993). The majority of the new MTFs improved upon CMOD3 and at least three variants gave very similar overall performances. After discussions with the contributors and ESA, a modified ECMWF model was recommended; this was similar in form to CMOD3 but had better-tuned coefficients. It was implemented as CMOD4 for operational use by ESA from 24 February 1993. This model is expected to remain the operational FD version for at least the remaining lifetime of *ERS-1*. The formulation of CMOD4 and its coefficients are presented in the appendix; its derivation is described by Stoffelen and Anderson (1993).

Figure 6 is a graph showing the performances of the three sequential versions of the operational FD models—CMOD2, CMOD3, and CMOD4—in retrieving wind speed when compared with the RENE-91 analyzed winds. The upper-left graph shows the speed bias and the upper right the SD, both as functions of BG wind speed, when averaged over all incidence angles. The lower graphs similarly show the speed bias (left) and SD (right) as a function of incidence angle, when averaged over wind speeds greater than 4 $m\ s^{-1}$. Figure 7 shows equivalent graphs for differences in wind direction.

The following significant features may be seen from these plots:

(i) The wind speed biases and their trends, both with wind speed and with incidence angle, have been much improved by CMOD4.

(ii) The wind speed SDs are also now significantly lower than the CMOD2 retrievals and are below 2 $m\ s^{-1}$ in nearly all bins.

(iii) As might be expected, there is a trend in all models from large wind direction SDs at very low wind speeds to smaller differences at high wind speeds, though the biases are increasing. However, we should note that there was only one *ERS-1* overpass in the RENE-91 collocation set with winds in excess of 20 $m\ s^{-1}$ and differences over cells in any single case are highly correlated.

(iv) There are also systematically larger differences in wind direction at low incidence angles (inner edge of the swath) for CMOD2 that are improved but not cured by CMOD4. This may indicate a physical limitation in the radar backscatter sensitivity to relative wind direction, and future scatterometers, such as the advanced scatterometer (ASCAT), are now being designed with their swaths offset to higher incidence angles (Miller et al. 1992).

(v) Except at low wind speeds and at the inner edge of the swath, the wind direction retrievals are within 20°.

Table 1 summarizes the performances of the old (CMOD2), interim (CMOD3), and current (CMOD4) models in terms of differences from the RENE-91 analyses, and Table 2 similarly for an extended validation against operational NWP fields. These results clearly show the overall improvements obtained by tuning the wind vector–σ^0 relationship.

To assess the quality of the *ERS-1* winds against the "true" wind—as assumed in the instrument specification—we have rerun the statistical analysis, using the CMOD4 retrievals versus the RENE-91 fields but applying different QI thresholds. The results are presented in Table 3. These results show that as the QI threshold is raised, there is a consistent improvement in the agreements. Since the formulation of CMOD4 was totally independent of the RENE-91 campaign data, we may conclude the following:

(i) The QI index is an indicator of the accuracy of the RENE-91 wind analyses; to obtain high QI values, the in situ data must have been spatially dense, be from several sources that mutually agree, and be close to the satellite overpass time.

(ii) Using a subset of only the very best quality analyzed winds (QI > 90) gives an agreement with the scatterometer-derived winds to 1.5 $m\ s^{-1}$ and 8° rms. However, we should note the small number of cells, and that this threshold resulted in the exclusion of all wind speeds above 20 $m\ s^{-1}$. There is also a suggestion (not shown) that the scatterometer winds are biased low above 16 $m\ s^{-1}$ by about 1.5 $m\ s^{-1}$ (but on a sample of only 30 cells). (This is also evident in larger

TABLE 3. As for Table 1 but for CMOD4 only, and varying the QI threshold below which cells are rejected.

QI threshold	Number of cells	Speed ($m\ s^{-1}$) Bias	Speed ($m\ s^{-1}$) SD	Direction (deg) Bias	Direction (deg) SD	Vector ($m\ s^{-1}$) rms
5	18 878	0.1	1.9	−1.6	17.0	3.2
10	12 232	0.1	1.9	−2.1	15.0	3.0
25	6999	0.1	1.7	−1.6	13.8	2.7
50	3547	0.1	1.6	−1.5	11.5	2.4
90	289	−0.1	1.5	−2.0	8.0	2.0

comparisons with NWP fields; it is suspected that this bias may arise because of the mismatch between the resolutions of global NWP analyses and the scatterometer footprints and the sparse data that they have available for assimilation.)

(iii) Given the above estimate of the scatterometer accuracy against "truth," the full RENE-91 analysis dataset itself can be assigned a share of the overall variance (with QI > 5) amounting to about 1.3 m s^{-1} and 15° rms.

(iv) Given that this subset is indeed highly representative of the true wind on the scale of the scatterometer footprint, and at the exact overpass time, then the instrument specification of 2 m s^{-1} and 20° rms has clearly been met. Also, it is clear that the dedicated RENE-91 campaign and the data analysis described in this paper has resulted in a high-quality dataset that exceeds the accuracy that could be expected of conventional [voluntary observing fleet (VOF) and NWP] data.

Putting these findings into context with "traditional" observations, Kent et al. (1993) have analyzed two years' worth of data from a specially selected set of VOF ships plying the North Atlantic. Most of the VOF use visual estimates of sea state and convert to wind speed using the Beaufort scale, while about one-third of the ships use either a fixed or hand-held anemometer. Overall, this study finds that the VOF wind observations, compared with the U.K. Meteorological Office's limited area model analyses (grid size approximately 80 km) had mean differences (observation minus model) of +1.5 m s^{-1} and were within ±5° for the majority of the ships. Standard deviations were of the order of 2.5 m s^{-1} and 10°. However, it should be noted that many of these observations will have been used in the NWP assimilation, so the datasets are to some extent correlated.

7. Conclusions

The RENE-91 campaign has provided a high-quality set of wind measurements from aircraft, ships, and buoys, which have enabled us to construct analysis fields covering a three-month period. We believe these fields to be the best available estimate of the true wind that can be used to compare with those from the *ERS-1* satellite, albeit limited in area and lacking in the higher wind speeds. These and other data sources have been used by other groups to "tune" the empirical relationship, or "model," between the near-surface wind vector and satellite radar backscatter measurements.

We have independently evaluated several candidate models by using a common retrieval scheme on the same data (primarily the RENE-91 collocated scatterometer measurements and analyses, and also daily fast-delivery products against operational NWP wind fields). One of the interim model transfer functions was recommended to ESA, which replaced the prelaunch model in their operational "fast-delivery" products for the latter half of 1992. Further tuning by the groups involved has resulted in a new model with significantly better performance, and ESA has been using this model since February 1993. Using a subset of the RENE-91 data, which is taken to most closely represent the "true" neutral-stability wind conditions at a height of 10 m, the scatterometer-derived winds using this model agree to 1.5 m s^{-1} and 8° rms—that is, better than specification, and a significant improvement upon conventional surface wind measurements.

In the future, small improvements (by modifying the empirical functional form and/or tuning the model's coefficients) may still be possible, but these will probably not be worthwhile implementing in ESA's operational system. Effort is now turning to improve the complete wind retrieval scheme and ambiguity removal algorithms—originally developed some years ago—to reflect the characteristics of the new model. For instance, in prelaunch simulations, the CMOD2 MTF, based on aircraft scatterometer measurements, was able to discriminate upwind–downwind ambiguities in most cases. In practice, the differences in the satellite-measured σ^0's are much smaller, making successful ambiguity removal more dependent on some prior knowledge of the general wind direction—as is already the case in the Meteorological Office's scheme. Looking even further into the future, the use of "neural networks"—which may be able to learn how to relate the σ^0 measurement directly to a single wind vector and/or which can recognize patterns for ambiguity removal—might be able to provide a means of bypassing the need for a fixed, explicit model and external knowledge of the general wind flow. Initial studies are already in progress to assess the feasibility of this approach.

Acknowledgments. I would like to thank the RAF aircrew of the C-130, the MRF staff, and all other RENE-91 participants for their invaluable help in making that campaign such a success, including the ESA representatives who provided the campaign support and excellent access to the *ERS-1* data, and Oceanor for the use of their facilities in Trondheim. My thanks are also extended to all of the analysis team participants for providing their model formulations and update coefficients to meet the deadlines placed upon the study.

APPENDIX

The CMOD4 Model Transfer Function

The CMOD4 model transfer function devised by Stoffelen (1993) is the current version used in the ESA fast-delivery processing of the *ERS-1* scatterometer. It is defined as

$$\sigma^0_{\text{lin}} = b_0(1 + b_1 \cos\phi + b_3 \tanh b_2 \cos 2\phi)^{1.6},$$

where $b_0 = b_r 10^{\alpha+\gamma\mathcal{F}_1(U+\beta)}$ and

$$\mathcal{F}_1(y) = \begin{cases} \sqrt{y}/3.2, & \text{if } y > 5 \\ \log_{10} y, & \text{if } 0 < y \leq 5 \\ -(\alpha + 6)/\gamma, & \text{otherwise;} \end{cases}$$

where U is the wind speed (m s^{-1}) and ϕ is the wind direction relative to the radar look azimuth angle. In this form, σ^0_{lin} is in linear measure; to convert to decibels:

$$\sigma^0_{\text{dB}} = 10 \log_{10} \sigma^0_{\text{lin}};$$

α, β, γ, b_1, b_2, and b_3 are expanded as Legendre polynomials to a total of 18 coefficients. Here, b_r is a residual correction factor to b_0 and is given as a look-up table (LUT) as a function of incidence angle:

$$\alpha = c_1 P_0 + c_2 P_1 + c_3 P_2$$

$$\gamma = c_4 P_0 + c_5 P_1 + c_6 P_2$$

$$\beta = c_7 P_0 + c_8 P_1 + c_9 P_2$$

$$b_1 = c_{10} P_0 + c_{11} U + (c_{12} P_0 + c_{13} U)\mathcal{F}_2(x)$$

$$b_2 = c_{14} P_0 + c_{15}(1 + P_1)U$$

$$b_3 = 0.42[1 + c_{16}(c_{17} + x)(c_{18} + U)]$$

$$b_r = \text{LUT}(\theta)$$

$$\mathcal{F}_2(x) = \tanh[2.5(x + 0.35)] - 0.61(x + 0.35),$$

where the Legendre polynomials in x are $P_0 = 1$, $P_1 = x$, $P_2 = (3x^2 - 1)/2$, with $x = (\theta - 40)/25$, where θ is the incidence angle from the local vertical, in degrees. The values for the coefficients $c_1 \cdots c_{18}$ and the look-up table for b_r are given in Tables A1 and A2.

TABLE A1. Legendre polynomial expansion coefficients for CMOD4.

Coefficient		Value
α	c_1	−2.301523
	c_2	−1.632686
	c_3	0.761210
γ	c_4	1.156619
	c_5	0.595955
	c_6	−0.293819
β	c_7	−1.015244
	c_8	0.342175
	c_9	−0.500786
b_1	c_{10}	0.014430
	c_{11}	0.002484
	c_{12}	0.074450
	c_{13}	0.004023
b_2	c_{14}	0.148810
	c_{15}	0.089286
b_3	c_{16}	−0.006667
	c_{17}	3.000000
	c_{18}	−10.000000

TABLE A2. Look-up table of residual corrections b_r to the b_0 term of CMOD4 as a function of incidence angle θ.

θ°	b_r	θ°	b_r
16	1.075	39	0.988
17	1.075	40	0.998
18	1.075	41	1.009
19	1.072	42	1.021
20	1.069	43	1.033
21	1.066	44	1.042
22	1.056	45	1.050
23	1.030	46	1.054
24	1.004	47	1.053
25	0.979	48	1.052
26	0.967	49	1.047
27	0.958	50	1.038
28	0.949	51	1.028
29	0.941	52	1.016
30	0.934	53	1.002
31	0.927	54	0.989
32	0.923	55	0.965
33	0.930	56	0.941
34	0.937	57	0.929
35	0.944	58	0.929
36	0.955	59	0.929
37	0.967	60	0.929
38	0.978		

REFERENCES

Attema, E. P. W., 1986: An experimental campaign for the determination of the radar signature of the ocean at C-band. *Proc. Third International Colloquium on Spectral Signatures of Objects in Remote Sensing,* Les Arcs, France, ESA, SP-247, 21–28.

——, 1991: The active microwave instrument on board the *ERS-1* satellite. *Proc. IEEE,* **79,** 791–799.

Axford, D. N., 1968: On the accuracy of wind measurements using an inertial platform in an aircraft and an example of the measurement of vertical meso-structure of the atmosphere. *J. Appl. Meteor.,* **7,** 645–666.

Battrick, B., and D. Guyenne, Eds., 1991: *ESA Bulletin. ERS-1* Special Issue, **65,** ESA, Noordwijk, the Netherlands.

Brown, R. A., V. J. Cardone, T. Guymer, J. Hawkins, J. E. Overland, W. J. Pierson, S. Peteherych, J. C. Wilkerson, P. M. Woiceshyn, and M. Wurtele, 1982: Surface wind analyses for Seasat. *J. Geophys. Res.,* **87**(C5), 3355–3364.

Cavanié, A., and D. Offiler, 1986: ERS-1 wind scatterometer: wind extraction and ambiguity removal. *Proc. IGARSS '86; Todays Solutions for Tomorrows Information Needs,* Zurich, Switzerland, ESA, SP-254, 395–398.

Chi, C.-Y., and F. K. Li, 1988: A comparative study of several wind estimation algorithms for spaceborne scatterometers. *IEEE Trans. Geosci. Rem. Sens.,* **GE-26,** 115–121.

Daniault, N., M. Champagne-Philippe, M. Camblan, and J. N. Thépaut, 1988: Comparison of sea surface wind measurements obtained from buoys, aircraft and on shore masts during the TOSCANE-T campaign. *J. Atmos. Oceanic Technol.,* **5,** 385–404.

ESA, 1988: Radar backscattering in the tropical rain forest. *Earth Observation Quarterly,* No. 21, ESA Publications, Noordwijk, the Netherlands, 6–7.

Ezraty, R., 1985: Study of an algorithm for the estimation of wind speed at the sea surface. IFREMER report to ESA, Contract 6155/85/NL/BI (in French).

Grantham, W. L., E. M. Bracalente, W. L. Jones, and J. W. Johnson, 1977: The Seasat-A satellite scatterometer. *IEEE J. Oceanic Eng.*, **OE-2**(2), 200–206.

Hayden, C. M., and R. J. Purser, 1988: Three-dimensional recursive filter objective analysis of meteorological fields. *CIMSS View,* **IV**(1), University of Wisconsin, Madison, WI.

Hunt, J. J., Ed., 1986: ERS-1 wind and wave calibration workshop. *Proc. ESA Workshop* Schliersee, Germany, ESA, **SP-262.**

Jones, W. L., and L. C. Schroeder, 1978: Radar backscatter from the ocean: dependence on surface friction velocity. *Bound.-Layer Meteor.*, **13,** 133–149.

Kent, E. C., P. K. Taylor, B. S. Truscott, and J. S. Hopkins, 1993: The accuracy of voluntary observing ship's meteorological observations—Results of the VSOP-NA. *J. Atmos. Oceanic Technol.*, **10,** 591–608.

Large, W. G., and S. Pond, 1982: Sensible and latent heat flux measurements over the ocean. *J. Phys. Oceanogr.*, **11,** 324–336.

Long, A. E., 1986: Towards a C-band radar sea echo model for the ERS-1 scatterometer. *Proc. Third International Colloquium on Spectral Signatures of Objects in Remote Sensing,* Les Arcs, France, ESA, **SP-247,** 29–34.

Long, M. W., 1988: *Radar Reflectivity over Land and Sea.* Lexington Books.

Miller, D., H. Ebner, P. Hans, H. Hölzl, and H. R. Schulte, 1992: An advanced scatterometer for the European polar platform. *Proc. Central Symposium of the 'International Space Year' Conference,* Munich, Germany, ESA, **SP-341,** 1153–1157.

Offiler, D., 1984: A comparison of Seasat scatterometer-derived winds with JASIN surface winds. *Int. J. Remote Sensing,* **5,** 365–378.

——, 1985: Wind direction ambiguity suppression algorithms. *Proc. The Use of Satellite Data in Climate Models,* Alpbach, Austria, ESA, **SP-244,** 175–176.

——, 1992: Validation and comparison of alternative wind scatterometer models. *Proc. ERS-1 Geophysical Validation Workshop,* Penhors, France, ESA, **WPP-36,** 125–132.

Readings, C. J., 1985: The use of aircraft to study the atmosphere: The Hercules of the Meteorological Research Flight. *Meteor. Mag.*, **114,** 66–77.

Schroeder, L. C., D. H. Boggs, G. J. Dome, I. M. Halberstam, W. L. Jones, W. J. Pierson, and F. J. Wentz, 1982: The relationship between wind vector measurements and normalised radar cross section used to derive Seasat-A satellite scatterometer winds. *J. Geophys. Res.*, **87**(C5), 3318–3336.

Stoffelen, A., and D. L. T. Anderson, 1993: ERS-1 scatterometer data characteristics and wind retrieval skill. *Proc. First ERS-1 Symposium—Space at the Service of our Environment,* Cannes, France, ESA, **SP-359,** 41–48.

Wentz, F. J., S. Peteherych, and L. A. Thomas, 1984: A model function for ocean radar cross sections at 14.6 GHz. *J. Geophys. Res.*, **89,** 3689–3704.

Wismann, V., 1992: Wind measurements over the ocean with an airborne C-band scatterometer during the ERS-1 calibration and validation campaign. *Proc. ERS-1 Geophysical Validation Workshop,* Penhors, France, ESA, **WPP-36,** 5–9.

——, 1993: A C-band wind scatterometer model derived from data obtained during ERS-1 calibration/validation campaign. *Proc. First ERS-1 Symposium—Space at the Service of our Environment,* Cannes, France, ESA, Paris, **SP-359,** 55–59.

Woiceshyn, P. M., M. G. Wurtele, D. H. Boggs, L. F. McGoldrick, and S. Peteherych, 1986: The necessity for a new parameterization of an empirical model for wind/ocean scatterometry. *J. Geophys. Res.*, **91,** 2273–2288.

Wooding, M., Ed., 1992: *Proc. ERS-1 Geophysical Validation Workshop,* Penhors, ESA, **WPP-36.**

Wu, J., 1982: Wind stress coefficients over sea from breeze to hurricane. *J. Geophys. Res.*, **87,** 9704–9706.